Characteristics of phosphate biosorption on nanoparticles of different woody-sawdust used for controlling P runoff and a supplemental P-fertilizer

Asmaa M. Ali[a], Ahmed M. Mahdy[a,*], Mohamed Z. Salem[b]

[a]Department of Soil and Water Sciences, College of Agriculture (Elshatby), Alexandria University, Alexandria 21545, Egypt, emails: amahdy73@yahoo.com/amahdy73@alexu.edu.eg (A.M. Mahdy), mahamedasmaa8@gmail.com (A.M. Ali)
[b]Department of Forestry and Wood Technology, College of Agriculture (Elshatby), Alexandria University, Alexandria 21545, Egypt, email: Zidan_forest@yahoo.com (M.Z. Salem)

ABSTRACT

To evaluate the potential of different woody sawdust nanoparticles (nSD) for phosphate biosorption capacity, a batch biosorption experiment was conducted on three types of sawdust nanoparticles. To achieve the objective, nanoparticles of the three types of woody-sawdust were produced by up-down method (ball mill mortar grinder) and phosphate solutions with various concentrations (5–320 mg/L), pHs, and temperatures were performed. The results revealed that the PO_4^{3-} sorption capacity of sawdust nanoparticle of Kafour tree (nSD-KF) was much higher than that of guava (nSD-GU) and Gohanamia (nSD-GH). The Langmuir model was the best fit to the experimental sorption data. The maximum adsorption capacity (q_{max}) value of nSD-KF (50,000 µg/g) for phosphate was higher than those of nSD-GU (33,300 µg/g) and nSD-GH (18,200 µg/g) sorbents, respectively. The first-order equation has been proved to be one of the best studied kinetic equations that capable of describing the sorption kinetics and sorption rate of phosphate onto the studied biosorbents. The solution pH greatly affected the charges of the active sites of nSD-KF and influenced the phosphate behavior in the solution. The phosphate sorption increased on the studied biosorbent with the increase of reaction temperature from 298 to 318 K, with constant of all other reaction conditions. The highest efficiency of phosphate removal by nSD-KF was at temperature of 318K at pHs normal and 7. The results of this study revealed that the ion exchange process, high specific surface area of nSD-KF, and ion complexation between phosphate and sawdust nanoparticles may be occurred in phosphate biosorption. The Fourier transform infrared analysis confirmed ion complexation between phosphate and sawdust nanoparticles depending on the chemical constituents of sawdust that containing many functional groups such as carboxylic, phenolic, hydroxyl, and carbonyl groups. In conclusion, the application of nanoscale sawdust particles in wastewater or wastewater-irrigated soils would substantially decrease P runoff and eutrophication. Moreover, the P-enriched nSD-KF may be used as a supplemental P-fertilizer required for plant growth to overcome high cost of mineral fertilizers applied to the agricultural soils.

Keywords: Nano-scale particles; Sawdust; Sorption; Water; Pollution; Eutrophication; Supplemental fertilizer

1. Introduction

The high phosphate contents in all types of wastewater especially agricultural wastewater resulted in deterioration of water quality through eutrophication [1]. Eutrophication of aqueous streams can be resulted from phosphorus runoff from agricultural soils and consequently hypoxia or anoxia conditions in waters [2]. Hence, removal of phosphate from polluted water by biodegradable sorbents and its use as a supplemental P-fertilizer are critical issues. Thus, new

* Corresponding author.

methods for removal of phosphate from wastewater before discharge into water bodies are required.

Biosorption is one of the most promising methods used for water quality treatment. Low-cost, availability, and biodegradability of materials used in the removal of phosphate from waters are limiting factors [3]. Use of biomaterials in phosphate removal from agricultural wastewater is known biosorption. Biosorption of phosphate from water will prevent its discharge into water bodies and subsequently eutrophication of water. The P-enriched biosorbents can be reused as compost or supplemental P-fertilizer for plant growth.

Biomaterials rich in ligno-cellulosic components, such as woody sawdust, are available, low-cost, and biodegradable and could be reused as a source of phosphate in the form of P-enriched compost after P saturation [4]. The broad potential of woody sawdust as biosorbent is due to its chemical constituents including easily available functional groups such as OH, COOH, NH_2, and phenols present in cellulose, lignin, hemicelluloses, alcohols, and aldehydes. Moreover, use of woody sawdust as phosphate biosorbent will allow simple separation between phosphate ions and biosorbent and its biodegradability would release more phosphate to agricultural soils when it is utilized as compost and supplemental P-fertilizer.

Recently, nanotechnology-based soil amendments that enable better control over the conditions for or timing of plant nutrients release were created. Nanoparticles have a huge reactive specific surface area [5] where tremendous quantities of phosphate can be sorbed [6]. The application of nanoscale sawdust particles in wastewater or wastewater-irrigated soils would substantially increase P sorption on amorphous nanoparticles and further decrease P runoff and eutrophication. It is necessary to define the soil and/or water conditions under which sawdust nanoparticles can be used beneficially and sustainably in an arid or semi-arid environment. In particular, the research on the interaction of sawdust particles with P is much necessary. The objectives of this study was to: investigate and characterize some chemical properties of sawdust nanoparticles (nSD) that produced from mechanically milling and the bulk sawdust collected; evaluate the potential of different woody sawdust nanoparticles for phosphate biosorption capacity; study the effect of pH and temperature on phosphate biosorption by sawdust nanoparticles; test fitness of kinetic and equilibrium models for experimental data; and investigate the possible mechanisms responsible for phosphate removal from water.

2. Materials and methods

2.1. Sampling of biomass and phosphate solution preparation

Bougainvillea spectabilis (stem wood), *Eucalyptus camaldulensis* L. (wood-branch), and *Psidium guaja* L. (wood-branch) were collected from Alexandria, Egypt during pruning processes. Bark of the woody species was removed, and the wood was transferred to flakes or sawdust in a sawmill in Alexandria.

Stock solution of 1,000 mg/L PO_4^{3-} was prepared using KH_2PO_4 salt. Different concentrations of phosphate solutions were prepared freshly prior to its use.

2.2. Producing and characterization of sawdust nanoparticles

The woody-sawdust was oven-dried at approximately 50°C–60°C, and then mechanically ground by a RETSCH RMl00 electrical mortar grinder (Ball mill) to produce nanoscale sawdust particles (diminish the particle size to <100 nm) according to the method of Elkhatib et al. [7].

The characteristics and element contents of all sawdust nanoparticles were investigated using scanning electron microscopy (SEM), and quipped with energy-dispersive X-ray spectroscopy (EDX). The surface structure of sawdust nanoparticles (nSD) was explored with Fourier transform infrared spectroscopy (FTIR) to illustrate the functional groups of the nanoparticle surfaces. The specific surface area of nanoparticles was determined using the method of Brunauer et al. [8]. All these measurements were carried out by standardized methods that have been routinely used for nanomaterial studies.

2.3. Batch biosorption experiments

Conducting biosorption experiments was performed by shaking 0.1 g of sawdust nanoparticles with 10 mL (1:100 ratio) of phosphate solutions with various concentrations (5, 10, 20, 40, 80, 160, and 320 mg/L) and pHs. The agitation was conducted at 400 rpm for 2 h to reach sorbate-sorbent equilibrium. At 0.5, 1, 2, 5, 10, 15, 20, 30, 40, 60, 90, and 120 min, aliquot was taken for phosphate kinetics determination. Then, centrifugation and filtration of supernatant were done. The filtrate was kept at 4°C for future analysis. Experiments were triplicated at a temperature of 25°C ± 3°C. At each time intervals (t), the amount of sorbed PO_4^{3-} ions by sawdust nanoparticles can be calculated from:

$$q = \frac{\left(\left(C_0 V_0\right) - \left(C_f V_f\right)\right)}{m} \tag{1}$$

where C_0 and C_f (mg/L) are the initial and final PO_4^{3-} concentrations, respectively, V is the volume of PO_4^{3-} solution (L), and m is the weight of the sawdust nanoparticles (g).

The PO_4^{3-} concentrations were determined calorimetrically according to ammonium–molybdate blue method [9].

The effect of hot water extraction method and solution pH on phosphate biosorption by sawdust nanoparticles was studied by various pH values ranged from 7 to 11. The 0.1 M HCl and NaOH solutions were used for reach to desired pH.

To assess quantitatively and qualitatively the adsorption efficiency of the sawdust nanoparticles, the most famous isotherm models (Langmuir, Freundlich, Temkin, Elovich, Fowler–Guggenheim, Kiselev, and Hill–de Boer) were investigated. Moreover, the most well-known kinetic models (power function, parabolic diffusion, first order, and Elovich) were used to test the fitness of experimental data. Both determination coefficient (R^2) and standard error of estimate (SE) were the basis to select the best-fit model.

FTIR analysis was used before and after hot water extraction of un-saturated and phosphate-saturated nSD-KF [10] to identify possible modifications of active sites in sawdust during element adsorption. The wavenumbers of FTIR were in the range of 400–4,000 cm^{-1}.

The effect of different temperatures (298, 308, 318 K) on phosphate biosorption by nSD-KF was studied.

2.4. Data and statistical analyses

Data and statistical analyses were done using the Statistical Analysis System (SAS Inc.).

3. Results and discussion

3.1. Sorption isotherm and kinetics of phosphate on sawdust nanoparticles

To evaluate and select the most appropriate sorbent or biosorbent and the optimum experimental conditions, sorption isotherms were used [11]. The sorption isotherm gives the equilibrium relationship between the concentration of phosphate at equilibrium and amount of sorbed phosphate by sawdust nanoparticles [12]. In this work, sorption isotherms were carried out to determine the sorption capacity for the three different types of nSD [nSD-KF (Kafour), nSD-GU (Guava), and nSD-GH (Gohanammia)] at initial concentrations range 5–320 mg/L (Fig. 1). Fig. 1 shows phosphate sorption by nSD-KF, nSD-GU, and nSD-GH as a function of phosphate concentration. A continuous increase of sorbed PO_4^{3-} by nSD-KF, nSD-GU, and nSD-GH with increasing PO_4^{3-} concentration from 5 to 320 mg/L is noticed and the PO_4^{3-} sorption capacity of nSD-KF was much higher than that of nSD-GU and nSD-GH (nSD-KF > nSD-GU > nSD-GH). It is interesting to note that the shape of nSD-KF sorption isotherm is an "*H*" type isotherm at low concentrations of phosphate [13] which reflects strong interaction between PO_4^{3-} and the nSD-KF adsorbent while, the shape of PO_4^{3-} sorption isotherm by nSD-GU and nSD-GH were *L*-type isotherms indicating intermediate affinity for PO_4^{3-} in comparison to nSD-KF.

For reliable prediction of PO_4^{3-} sorption parameters on the studied sorbents (nSD-KF, nSD-GU, and nSD-GH), the preceding seven sorption isotherm models were employed (Table 1). Higher R^2 and smaller SE values indicate best-fitting of the model predictions with the experimental
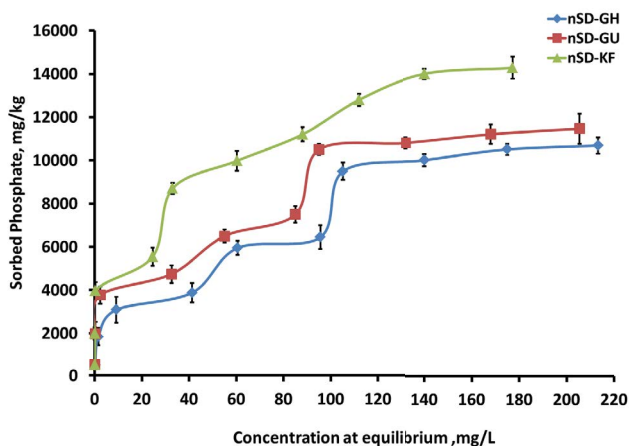
data [14]. The data of Table 1 demonstrated that Langmuir and Freundlich were successful in describing PO_4^{3-} sorption data by the three biosorbents studied as evidenced by high R^2 and Low SE values.

3.1.1. Langmuir isotherm model

Table 1 and Fig. 2 show the description of the PO_4^{3-} sorption on nSD-KF, nSD-GU, and nSD-GH by the linear form of Langmuir isotherm model. The R^2 and SE values for Langmuir model ranged from 0.99 to 0.98 and 0.0005 to 0.0001, respectively for PO_4^{3-} by nSD-KF, nSD-GU, and nSD-GH (Fig. 2; Table 1). The SE values calculated by Langmuir model for PO_4^{3-} sorption on the sorbents studied were much lower compared to the other six sorption isotherm models used (Table 1). Therefore, the Langmuir model was the best fit to the experimental sorption data suggesting that the PO_4^{3-} removal from the surface of nSD-KF, nSD-GU, and nSD-GH sorbents was monolayer mode of adsorption. The maximum adsorption capacity (q_{max}) value of nSD-KF (50,000 µg/g) was higher than those of nSD-GU (33,300 µg/g) and nSD-GH (18,200 µg/g) sorbents, respectively (Table 1). In comparison with bulk sawdust, the q_{max} of nanoparticles was 10–15 times of bulk particles (SD-KF = 3,000 µg/g; SD-GU = 2,200 µg/g; SD-GH = 1,600 µg/g). This is surprising since the specific surface area of nSD-GU (14.58 m²/g) is higher than the specific surface area of nSD-KF (11.33 m²/g), and nSD-GH (9.72 m²/g). This is indicating that there was another sorption mechanism in addition to SSA involved in sorption of PO_4^{3-} on nSD-KF. The Langmuir K_L values of PO_4^{3-} for nSD-KF sorbent was much higher than K_L values of nSD-GU and nSD-GH sorbents (Table 1).

3.1.2. Freundlich isotherm model

Phosphate sorption was fitted to the Freundlich equation for all the sorbents with R^2 ranging from 0.85 to 0.97. Freundlich isotherm parameters were calculated from the slope and intercept of the linear equation form and are shown in Table 1. The higher values of K_F reflect a large sorption capacity of the biosorbents for PO_4^{3-} [15]. Data in Table 1 shows that the highest Freundlich K_F value of the sorbents was for nSD-KF (3,498.19 mL/g) and the lowest was for nSD-GH (1,187.97 mL/g). It is clear that modifying bSD-KF to nanoparticles greatly increased its capability for PO_4^{3-} removal. The $1/n$ values of Freundlich isotherm were within a narrow range (0.26–0.38) for the three studied sorbents and reflect the observed similarities of the overall shape of PO_4^{3-} isotherms as shown in Fig. 2. The Freundlich model successfully described PO_4^{3-} sorption at concentration range of 5–320 mg/L. However, the SE values calculated by Freundlich model for PO_4^{3-} sorption on the sorbents studied were much higher than those of Langmuir model which indicate the superiority of Langmuir model over Freundlich model in describing PO_4^{3-} sorption by the biosorbents studied.

3.1.3. Biosorption kinetics

The kinetic experiments were performed to evaluate the sorption potential of the studied biosorbents and to determine the time required for PO_4^{3-} to reach maximum sorption

Fig. 1. Phosphate sorption isotherm of nSD-KF, nSD-GU, and nSD-GH biosorbents.

Table 1
Sorption isotherm model parameters for PO_4^{-3} on three sorbents and initial concentrations of 5–320 mg/L at 25°C

Models	Parameter	nSD-GU	nSD-KF	nSD-GH
Freundlich:	K_F (mL/g)	1,998.20	3,498.19	1,187.97
$q_e = K_F C_e^{1/n}$	$1/n$	0.33	0.26	0.38
	R^2	0.85	0.97	0.88
	SE	0.45	0.36	0.78
Langmuir:	q_{max} (µg/g)	33,300	50,000	18,200
$q_e = q_{max}(K_L C_e/1 + K_L C_e)$	K_L (L/mg)	0.18	0.30	0.07
	R^2	0.99	0.98	0.98
	SE	0.0005	0.0001	0.0001
Elovich:	q_{max} (µg/g)	2,000	2,500	1,670
$q_e/q_m = K_E C_{e,exp}(-q_e/q_m)$	K_E (L/mg)	3.70	55.23	0.62
	R^2	0.91	0.88	0.86
	SE	0.93	1.70	0.65
			70	
Temkin:	ΔQ (kJ/mol)	70.50	124	38.10
$\theta = RT/\Delta Q \ln K_0 C_e$	K_0 (L/g)	13.75	251.55	3.99
	R^2	0.89	0.93	0.88
	SE	0.03	0.035	0.046
Fowler–Guggenheim (FG)	W (kJ/mol)	27.27	2.16	4.57
$K_{FG} C_e = \theta/1 - \theta \exp(2\theta w/RT)$	K_{FG} (L/mg)	0.05	18.17	0.06
	R^2	0.91	0.85	0.78
	SE	0.92	2.03	0.87
Kiselev:	K_1 (L/mg)	0.07	16.20	0.14
$K_1 C_e = \theta/(1 - \theta)(1 + K_n \theta)$	K_n	−9.92	−6.22	−3.84
	R^2	0.99	0.98	0.99
	SE	0.49	100.48	0.37
Hill–deBoer:	K_1 (L/mg)	0.06	1.99	0.05
$K_1 C_e = \theta/(1 - \theta) \exp(\theta/(1 - \theta) - K_2\theta/RT)$	K_2 (kJ/mol)	−62.40	−26.90	−2.40
	R^2	0.92	0.79	0.26
	SE	0.92	2.07	0.95

q_e (mg/g) is phosphate adsorbed per gram of adsorbent, C_e (mg/L) is equilibrium phosphate concentration in solution, K_F is a constant related to adsorption capacity of the adsorbent (L/mg), n is a constant, q_{max} (mg/g) is the maximum adsorption capacity of the adsorbent, K_L (L/mg) is Langmuir constant related to the free energy of adsorption, θ is fractional coverage, R is the universal gas constant (kJ/mol/K), T is the temperature (K), ΔQ is ($-\Delta H$) the variation of adsorption energy (kJ/mol), K_0 is Temkin constant (L/g), K_{FG} is Fowler–Guggenheim constant (L/mg), W is the interaction energy between adsorbed molecules (kJ/mol), K_1 is Kiselev constant (L/mg), K_n is a constant of complex formation between adsorbed molecules, K_1 is Hill–de Boer constant (L/mg), and K_2 (kJ/mol) is a constant related to the interaction between adsorbed molecules. A positive K_2 means attraction between adsorbed species and a negative value means repulsion.

on nSD-KF, nSD-GU, and nSD-GH. For 80 mg/L PO_4^{3-} solution, it was noted that the maximum PO_4^{3-} removed by nSD-KF, nSD-GU, and nSD-GH were 69%, 59%, and 49%, respectively as the equilibrium reached after 2 h. However, for 160 mg/L PO_4^{3-} solution, it was noted that the maximum PO_4^{3-} removed by nSD-KF, nSD-GU, and nSD-GH were 63%, 50%, and 41%, respectively. For economical wastewater treatment application, equilibrium time is an important parameter. So, these data are important [16]. In the sorbents studied, the sorption kinetics of PO_4^{3-} exhibited an immediate rapid sorption by which about 96%–99% of PO_4^{3-} was sorbed in the first 10 min and followed by slow sorption at 298 K (Fig. 3). The rapid initial adsorption of PO_4^{3-} was due to rapid filling up of sorption sites on sawdust nanoparticles with PO_4^{3-} ions in the initial stages and followed by a slow migration and diffusion because limited numbers of active

sites. The amount of PO_4^{3-} sorbed per unit mass of biosorbent increases with the increase of PO_4^{3-} initial concentrations. For example, the amount of PO_4^{3-} removed at 120 min jumped from 5,545 to 9,977 µg/g, at 80 and 160 mg/L, respectively for nSD-KF (Fig. 3). Similarly, for nSD-GU the amount of PO_4^{3-} removed at 120 min jumped from 4,742 to 7,986 µg/g, at 80 and 160 mg/L, respectively (Fig. 3). Also, the amount of PO_4^{3-} removed at 120 min jumped from 3,877 to 6,442 µg/g, at 80 and 160 mg/L, respectively for nSD-GH (Fig. 3). The increase of initial concentration may enhance the interaction between the ions and the sorbent surface [17].

3.1.4. Sorption kinetic modeling

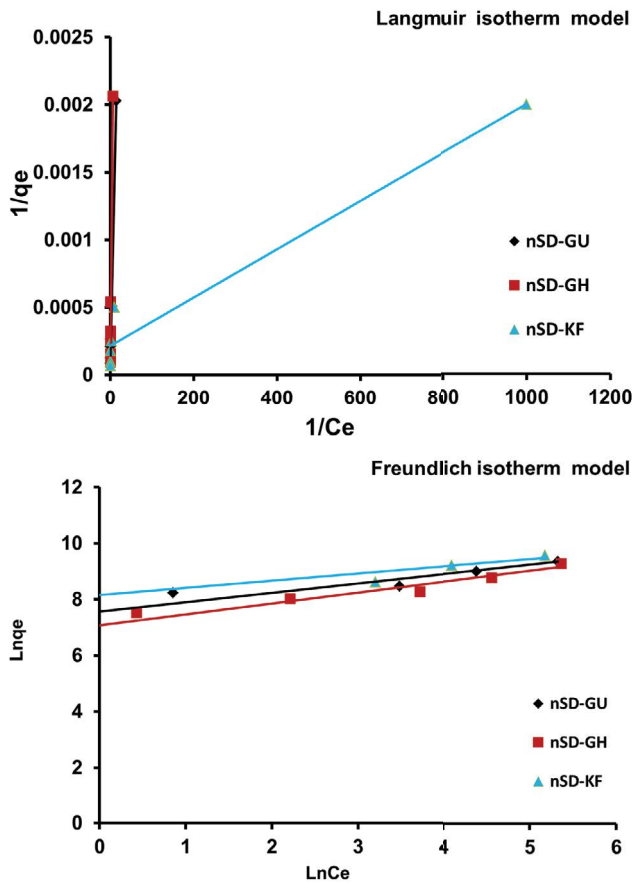The PO_4^{3-} sorption kinetics by the biosorbents studied (nSD-KF, nSD-GU, and nSD-GH) was performed and

Fig. 2. Langmuir and Freundlich isotherm models of phosphate biosorption onto nSD-KF, nSD-GU, and nSD-GH biosorbents.

Fig. 3. Effect of contact time on PO_4^{-3} sorption by nSD-KF, nSD-GU, and nSD-GH at initial PO_4^{-3} concentration of 80 and 160 mg/L at temperature of 298 K.

analyzed using first-order [18], Elovich [19], intraparticle diffusion model [20], and modified Fruendlich [21] kinetic models. To test the conformity between experimental and predicted data, the R^2 and SE values were used (Table 2). High R^2 and low SE values indicate the success of model in describing the kinetics of PO_4^{3-} sorption on biosorbents. It is important to select the best-fit model for data and agrees with the sorption mechanism of sorbate on biosorbent. Each model used in this study has a specific function. In general, the Elovich model was used to describe the kinetics of exchange reactions. Thus a plot of *q* vs. ln*t* should give a linear relationship with the slope of $(1/\beta)$ and intercept of $(1/\alpha)\ln(\alpha\beta)$ (Table 2). In the intra-particle diffusion model, a plot of "*q*" vs. $t^{1/2}$ should provide a linear relationship in case of the reaction conformity to parabolic diffusion law. In the power function model, the parameter K_a, C_0, and $1/m$ were obtained from the intercept and slope, respectively of the linear plots. Also, in the first order model, the "ln*q*" vs. "*t*" relationship is linear in case of conformity of sorption–desorption to first-order equation.

The kinetics model constants, R^2 and SE values for PO_4^{3-} sorption by nSD-KF, nSD-GU, and nSD-GH are given in Table 2. The highest values of R^2 for first order model for PO_4^{3-} were found to be 0.89, 0.87, and 0.86 for nSD-KF, nSD-GU, and nSD-GH, respectively, which were greater than the R^2 values of power function that were 0.86, 0.81,
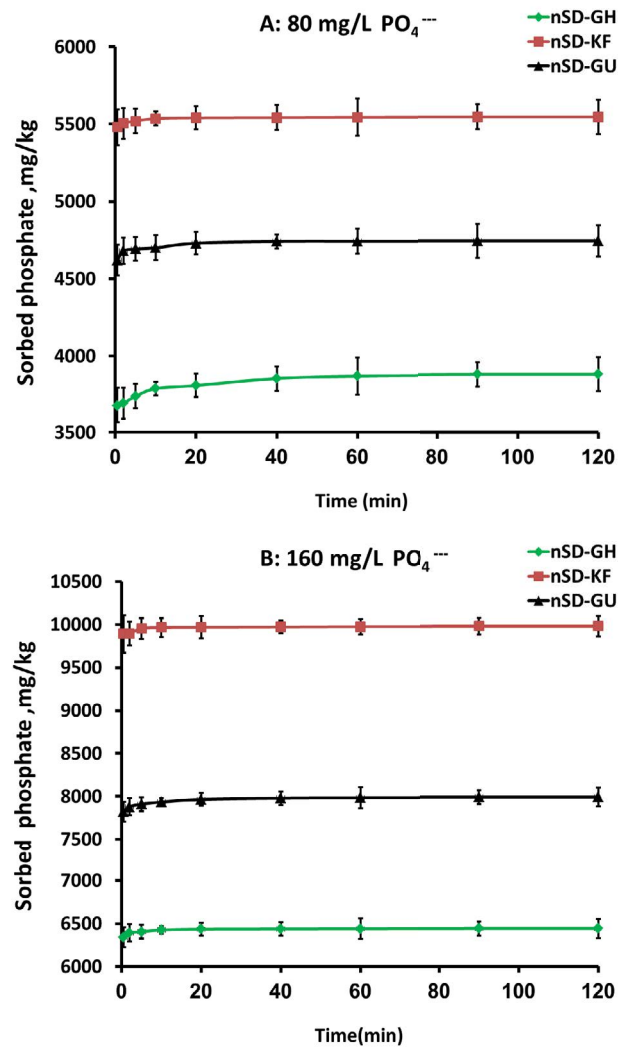
and 0.82 for nSD-KF, nSD-GU, and nSD-GH, respectively (Table 2). The R^2 values of Elovich and intraparticle diffusion models were much lower than R^2 of first-order model and SE values of Elovich and intraparticle diffusion models were quite high. Therefore, sorption kinetics data for nSD-GU, nSD-KF, and nSD-GH followed first order and power function models as confirmed by higher R^2, and lower SE values (Table 2) suggesting that the type of sorption mechanism could be chemical sorption [22].

3.2. Effect of initial PO_4^{3-} concentration on PO_4^{3-} biosorption

The first-order equation has been proved to be one of the best studied kinetic equations that capable of describing the sorption kinetics and sorption rate of PO_4^{3-} onto the nSD-KF, nSD-GU, and nSD-GH biosorbents as affected by initial PO_4^{3-} concentrations and this was confirmed by relatively high R^2 and low SE values (Table 2). On changing the PO_4^{3-} concentrations from 80 to 160 mg/L at 298 K, the K_a values increased for nSD-KF, nSD-GU, and nSD-GH

Table 2
Kinetics, model parameters, determination coefficients, and standard error of estimate for phosphate sorption by nSD-GU, nSD-KF, and nSD-GH biosorbents for 160 mg/L PO_4^{-3}

Models	Parameter	nSD-GU	nSD-KF	nSD-GH
Elovich	α, mg/g/min	8.9E+111	1E+253	4E+159
	β, mg/g	0.033	0.058	0.057
	R^2	0.96	0.83	0.89
	SE	10.20	15.59	11.37
First-order	K_a, 1/min	0.045	0.032	0.034
	a, µg/g	4.35	3.54	3.52
	R^2	0.87	0.89	0.86
	SE	0.0006	0.0007	0.0008
Intraparticle diffusion	K_a, µg/g/min$^{1/2}$	13.67	7.26	7.35
	a, µg/g	7,867.8	9,915	6,379.5
	R^2	0.73	0.58	0.62
	SE	30.36	24.07	22.58
Power function	K_a, 1/min	7,855.97	9,906.04	6,309.57
	$1/m$	0.004	0.002	0.003
	R^2	0.86	0.81	0.82
	SE	0.46 0.07	0.70	0.56

q = the amount of sorbate adsorbed per gram of adsorbent in time t.
α = the initial adsorption or desorption rate (mg/g/min).
β = a constant, related to the extent of surface coverage (mg/g) and activation energy for chemisorptions.
K_a = apparent sorption diffusion rate coefficient (µg/g/min$^{1/2}$).
C_0 = initial sorbate concentration (mg/L).
t = reaction time (min).
K_a = adsorption rate coefficient (1/min).
$1/m$ = a constant.
q_0 = amount of sorbate adsorption at equilibrium.

biosorbents (Table 3 and Fig. 4). For example, at 80 and 160 mg PO_4^{3-}/L concentrations, PO_4^{3-} sorption on nSD-KF, nSD-GU, and nSD-GH biosorbents at 298 K resulted in increases of K_a from 0.028 to 0.032, 0.033 to 0.045, and 0.026 to 0.034, respectively. It is obvious that the PO_4^{3-} concentration had a considerable effect on PO_4^{3-} sorption rate.

3.3. Characterization of high sorptive capacity-biosorbent (nSD-KF)

The X-ray diffraction (XRD) patterns of hot water extracted and not-extracted nSD-KF indicated that nSD-KF sample is mainly containing high percentage of nitrogen and phosphorus. Moreover, presence of amorphous materials was observed and this was due to the significant amount of lignin and cellulose (lingo-cellulosic biosorbent) found in nSD-KF. While, after hot water extraction, the nitrogen was disappeared but, phosphorus still found (Data not shown). Also, presence of amorphous materials was observed due to the sample still contain significant amount of lignin and cellulose. These results coincided with the results of Abdel-Rahman et al. [23], they reported that the presence of lignin in sawdust sample resulted in amount of amorphous material shown in XRD patterns.

SEM and EDX analyses of nSD-KF before and after phosphate saturation are shown in Figs. 5a and b. The SEM images of nSD-KF samples clearly showed that the representative single particle size dimension lies in the range 1–100 nm (nanostructure). After saturation with phosphate, a layer of sorbed phosphate on the nSD-KF surface was observed which ascertained adsorption of phosphate by nSD-KF (Fig. 5b). The elemental analysis of nSD-KF illustrated in Fig. 5 confirmed these results by appearance of phosphate (3.54%) peak in phosphate-saturated nSD-KF. Moreover, the size distribution of Zetasizer analysis refers to size average 98 nm (<100 nm).

The specific surface area (SSA) of nSD-KF (11.33 m^2/g) is much higher than that of the bulk bSD-KF sample (1.53 m^2/g). Indeed, the high SSA could supply nSD-KF with highly reactive sites for PO_4^{3-} sorption. These results coincided with the results of Wahab et al. [24] and Gogoi et al. [25], they reported that the untreated and unsieved sawdust have a lower surface area (1.43 m^2/g) than fine dusts. In addition, other observations were recorded on different materials such as moringa seed waste. Ajav and Fakayode [26], they reported that the value of specific surface area of bulk moringa seed waste was 177 mm^2/g. Also, Mnisi and Ndibewu [27] reported that SSA values of bulk moringa seed waste were 1.79 and 2.97 m^2/g, respetively.

The electric potential across the layer in the electric double-layer in soil called "zeta potential". The zeta potential value reflects the quantity of charges absorbed by the
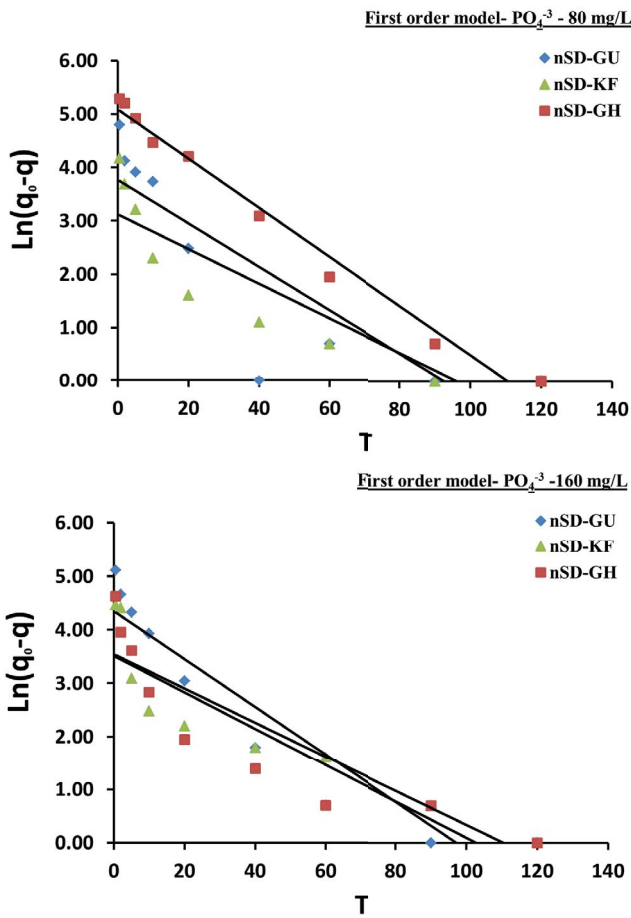
Fig. 4. First-order kinetic model for PO_4^{-3} sorption on nSD-KF, nSD-GU, and nSD-GH biosorbents as affected by initial PO_4^{-3} concentration.

Table 3
First-order-kinetics parameters of nSD-GU, nSD-KF, and nSD-GH biosorbents as affected by initial PO_4^{-3} concentration

Initial PO_4^{-3} Concentration	Parameter	nSD-GU	nSD-KF	nSD-GH
80 mg/L	K_a (1/min)	0.033	0.028	0.026
	a (µg/g)	3.76	3.12	5.09
	R^2	0.75	0.80	0.96
	SE	0.68	0.42	0.49
160 mg/L	K_a (1/min)	0.045	0.032	0.034
	a (µg/g)	4.35	3.54	3.52
	R^2	0.89	0.87	0.86
	SE	0.0006	0.0007	0.0008

solid [28–30]. Based on the above concept, the zeta potential characteristics of a nSD-KF was studied. The results of current study showed that zeta potential of sawdust nanoparticles of Kafour wood was –26.36 mV that indicating more surface charge on particles and increase the sorptive capacity of nSD-KF. Abidi et al. [31] conducted a study

on the removal of dye from industrial wastewater using clay particles as a sorbent at different values of zeta potential and reported that the measurements of zeta potential can be used in the determination of electrical charge and behavior of dyes at the clay-water interface.

3.4. Effect of hot water-extraction, temperature, and solution pH

The solution pH plays a crucial rule in the adsorption process, since. It greatly affects the charges of the active sites of nSD-KF and influence the phosphate behavior in the solution [32–34]. In this study, effect of initial pH on the biosorption process was monitored in the pH range of 7–11 for hot water-extracted and not-extracted nSD-KF (Fig. 6a) at the biosorbent dose of 0.1 g, initial concentration of 160 mg/L, and temperature of 298 K. The phosphate adsorption was highly influenced by solution pH (Fig. 6a). For the hot water-not extracted nSD-KF, the amount of sorbed phosphate at equilibrium was maximum (9,977 mg/kg) at normal pH and decreases to 9,474; 9,186; and 6,985 mg/kg at pH 7, 9, and 11, respectively.

On the other hand, for the hot water-extracted nSD-KF, the adsorbed phosphate amount at equilibrium was less than that of not-extracted nSD-KF at all pHs. The adsorbed phosphate amounts at equilibrium were 2,820; 2,160; 1,940; and 1,880 mg/kg at pH normal, 7, 9, and 11, respectively (Fig. 6a). The reduction in amount of sorbed phosphate at high pH values was due to the competition between phosphate ions and the other anions present at high pH.

In comparison of phosphate amount removed by hot water-extracted nSD-KF and not-extracted one, it is found that the amount of phosphate removed by not-extracted nSD-KF was significantly higher than that of extracted nSD-KF at all pHs (Fig. 6a). This large difference between extracted and not extracted at all pH values may be due to ion complexation between phosphate ion and functional groups present in nSD-KF composition. The dramatic changes in P sorption with increasing pH indicates that the chemisorption is the dominant mechanism in P-nSD-KF system. In general, variation in the removal of phosphate ions with respect to pH can be explained by considering surface properties of biosorbent material and ionization state of phosphate [35]. It is plausible that at low and neutral pHs, the nSD-KF surface is covered with hydronium ions (H⁺) that sorb phosphate ions and causing a high removal percentage. Increasing the pH may increase the repulsive forces between the negatively charged ions, causing a lower removal %. In addition, with the pH increase, the carboxylic groups present in sawdust are de-protonated due to the presence of high amount of negative charges, and the sorption process is reduced by the repulsion of the negative charges (ions). A similar trend has been observed for the adsorption of phosphate by biochar of sawdust [36] and nWTRs [7].

The effect of temperature on PO_4^{3-} sorption on nSD-KF biosorbent was studied at three different temperatures (298, 308, and 318 K) and 160 mg/L initial PO_4^{3-} concentration. As the temperature of the reaction increased from 298 to 318 K, with all other reaction conditions remaining constant, the PO_4^{3-} sorption increased on the studied biosorbent. The highest efficiency of PO_4^{3-} removal by nSD-KF was at temperature of 318 K at normal pH (Fig.
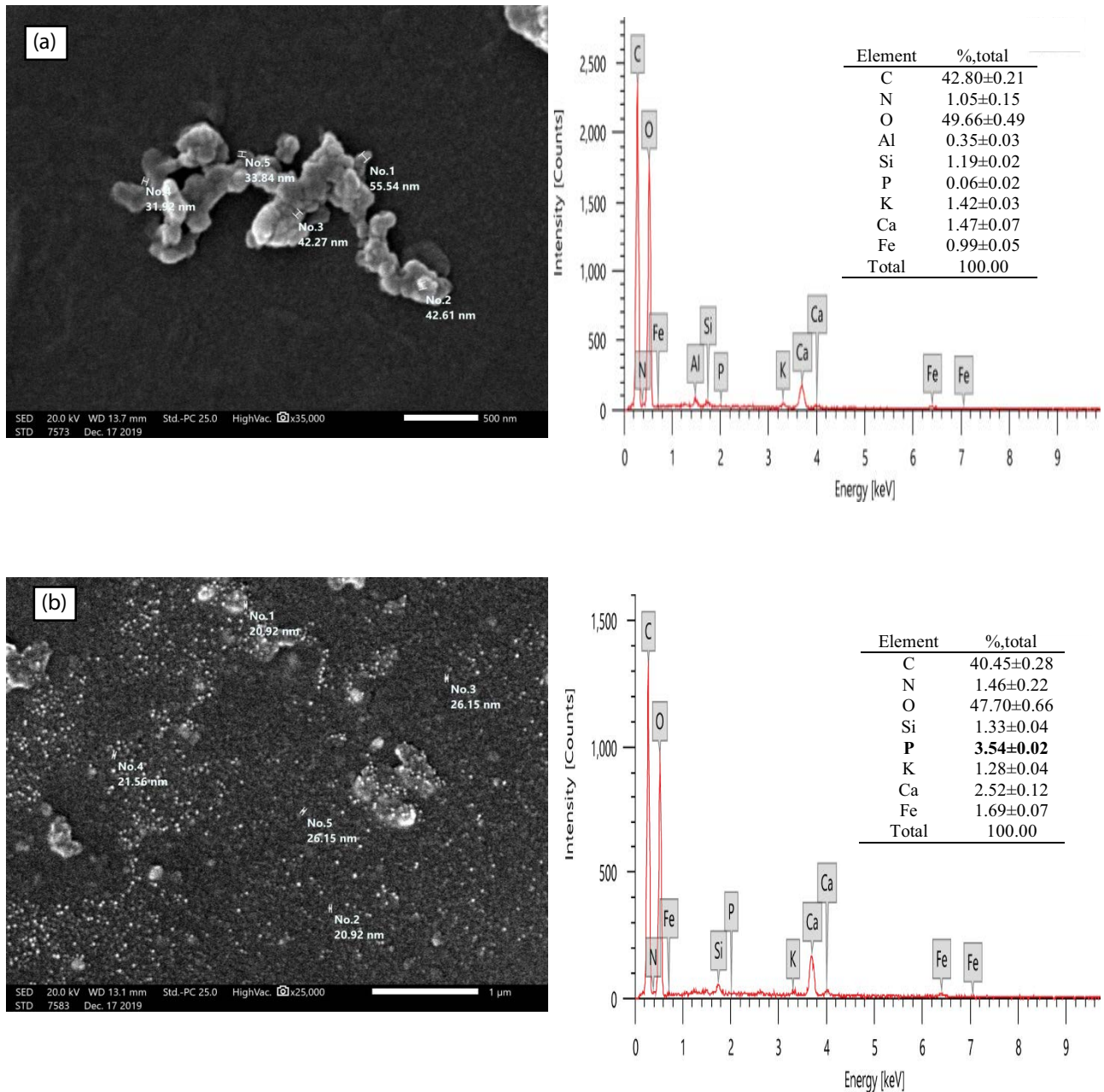
Element	%,total
C	42.80±0.21
N	1.05±0.15
O	49.66±0.49
Al	0.35±0.03
Si	1.19±0.02
P	0.06±0.02
K	1.42±0.03
Ca	1.47±0.07
Fe	0.99±0.05
Total	100.00

Element	%,total
C	40.45±0.28
N	1.46±0.22
O	47.70±0.66
Si	1.33±0.04
P	**3.54±0.02**
K	1.28±0.04
Ca	2.52±0.12
Fe	1.69±0.07
Total	100.00

Fig. 5. Scanning electron microscopy (SEM) image and energy dispersive X-ray (EDX) elemental distribution of nSD-KF ((a): un-saturated and (b): phosphate-saturated).

6b). The increase of phosphate sorption at higher temperature may be due to cellulose structure become open, mobility and penetration of phosphate through sawdust may be enhanced, and the activation energy barrier will be overcame and the rate of intra-particle diffusion will be enhanced [37]. There is, however, a limit for maximum temperature at which sorption of phosphate ions would be occurred and it is suggested to be 30°C–60°C. Bryant et al. [38] pointed out that sorption of heavy metals on sawdust was significant and the solubilization of wood extractives, like tannins, was high at 60°C. Tannins are serving as the primary site for ion binding to wood [39].

The results of this study were in agreement with the results of Raji et al. [40]; Anirudhan and Sreedhar [41] they studied the temperature effect on heavy metal sorption by sawdust materials and reported the increase of heavy metals biosorption with the increase in temperature. Jellali et al. [34] conducts an experiment to study the ammonium biosorption on *Posidonia oceanica* (L.) fibers and found that the amount of removed ammonium was affected by sorption operating parameters. Ismail et al. [42] studied the effect of temperature effect on cadmium ion removal by powdered corn cobs in batch experiments. They reported that there was an increase in Cd biosorption by the increase
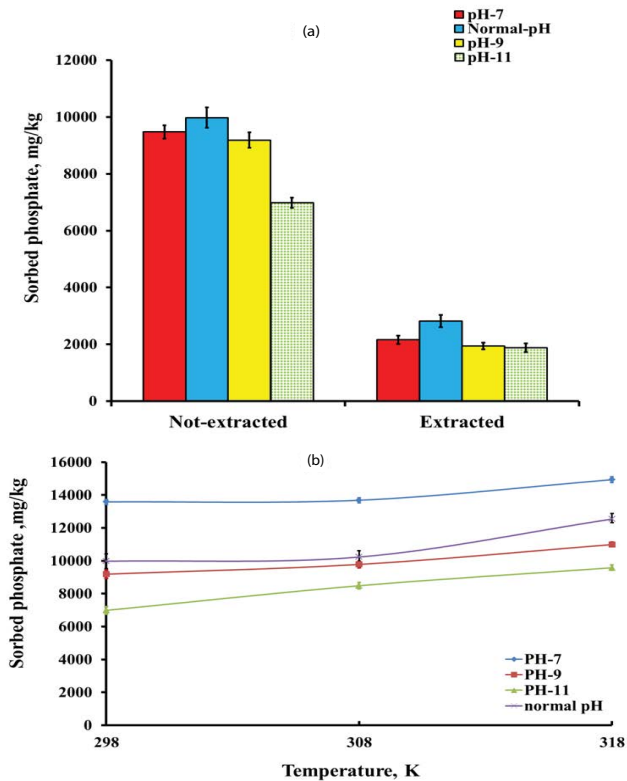
Fig. 6. Effect of (a) pH on PO_4^{-3} sorption by hot water-extracted and not-extracted nSD-KF at the equilibrium time of 2 h and temperature of 298 K and (b) temperature on PO_4^{-3} sorption by nSD-KF at the equilibrium time of 2 h and temperature of 298, 308, and 318 K.

of temperature from 25°C to 55°C. The q_{max} of the studied biosorbent was observed as 18.15 mg Cd/g at 25°C and 25.51 mg Cd/g at 55°C. The efficient removal of ions at high temperatures may be attributed to either increase of numbers and activity of sorption sites present on biosorbents or due to the decrease in the mass transfer resistance of ions as a result of decrease in boundary thickness of the layer surrounding the biosorbent. Fomina and Gadd [43] reported that the increase of surface activity and kinetic energy of sorbate occurred at high temperatures may cause the increase of biosorption rate of ion.

3.5. Probable mechanism of phosphate biosorption

The FTIR spectrum of nSD-KF before and after hot water-extraction for unsaturated and phosphate-saturated nSD-KF are shown in Fig. 7) that display peaks of absorption referring to a reaction occurred between phosphate ions and nSD-KF. The different characteristic peaks shown in Fig. 7 indicate to heterogeneity of nSD-KF biosorbent and presence of many functional groups as proton donors and their possible involvement with phosphate ions. To investigate the possible complexation between phosphate ions and nSD-KF, the FTIR spectra of hot-water extracted and not extracted nSD-KF before and after PO_4^{3-} saturation was compared (Fig. 7). After phosphate saturation either before or after extraction with hot water, shifting of some
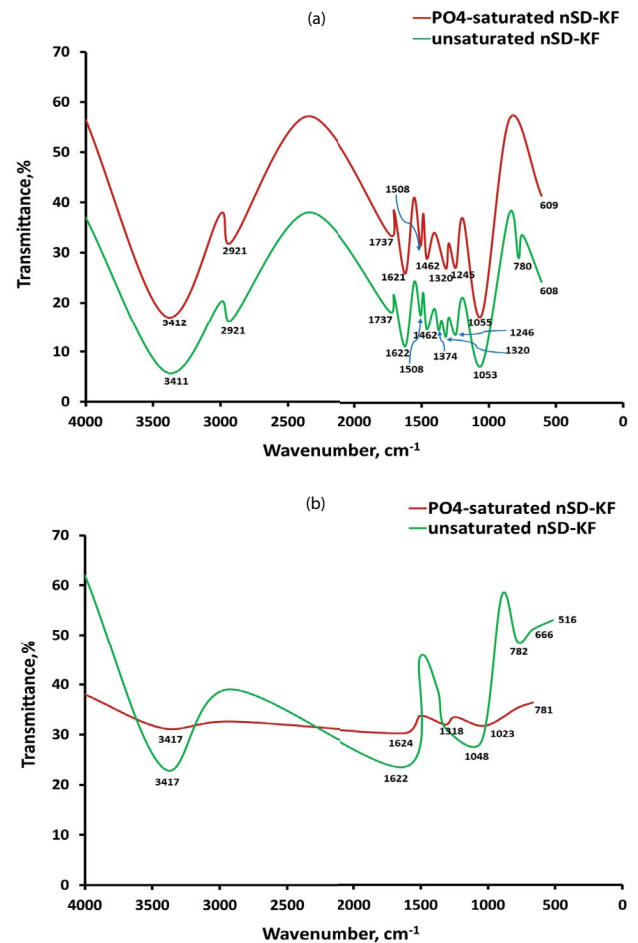

Fig. 7. Fourier transmission infrared (FTIR) spectra of (a) before and (b) after hot water-extraction of phosphate saturated-nSD-KF.

functional groups bands of nSD-KF was observed (Fig. 7). This was due to the possible changes of the ions present in some functional groups like carboxyl and hydroxyl, suggesting that they are involved in the complexation between PO_4^{3-} ions and sawdust biosorbent, and possibility of ion exchange between phosphates and counter ions.

Before hot water extraction, most band shifting or changes occurring on the nSD-KF after PO_4^{3-} saturation are shown between 1,700 and 500 cm⁻¹ wavenumbers which may be attributed to complexation of PO_4^{3-} and COOH group and bonded O–H bands of carboxylic acids present in alcohols, phenols pectin, cellulose, and lignin [44]. In addition to ion exchange and high specific surface area of nSD-KF, the ion complexation between phosphate and sawdust nanoparticles may be occurred in phosphate biosorption. The FTIR analysis confirmed this issue depending on that the chemical constituents of any plant residues contain many functional groups such as carboxylic, phenolic, hydroxyl, and carbonyl groups [45].

After hot water extraction, the FTIR spectrum before and after phosphate saturation was completely different and most observed changes were between 3,450 and 3,200 cm⁻¹ wavenumber which referred to ion complexation

of PO_4^{3-} with OH of alcohols and phenols in addition to carboxylate present in lingo-cellulosic materials [44]. The appearance of some minor changes in spectral bands, before and after phosphate biosorption on the sorbents, may be evident to ion exchange process [46]. Volesky [47] and Mahdy et al. [48] revealed that hydroxyl, carbonyl, and amine functional groups have been proposed to be responsible for metal binding and uptake by plant biomass via adsorption, coordination, chelation, complexation, and/or ion exchange. Thus, in the current study hydroxyl, carbonyl, and amine functional groups may be responsible for the biosorption properties of ammonium on nSD-KF (Fig. 7).

4. Conclusions

The results of this study revealed that the maximum adsorption capacity (q_{max}) value of nSD-KF for phosphate was higher (50,000 µg/g) than other sorbents (33,300 µg/g for nSD-GU and 18,800 µg/g for nSD-GH). Consequently, the maximum removal efficiency of PO_4^{3-} by nSD-KF was higher and reached to 94%. The solution pH and temperature played a crucial rule in the adsorption process, since they greatly affect the charges of the active sites of nSD-KF and influence the phosphate behavior in the solution. For the hot water-not extracted nSD-KF, the amount of sorbed phosphate at equilibrium was maximum (9,977 mg/kg) at normal pH and decreases to 9,474; 9,186; and 6,985 mg/kg at pH 7, 9, and 11, respectively. On the other hand, for the hot water-extracted nSD-KF, the adsorbed phosphate amount at equilibrium was less than that of not-extracted nSD-KF at all pHs. The adsorbed phosphate amounts at equilibrium were 2,820; 2,160; 1,940; and 1,880 mg/kg at pH normal, 7, 9, and 11, respectively.

According to FTIR and other analyses, the ion exchange process, high specific surface area of nSD-KF, and ion complexation between phosphate and sawdust nanoparticles may be occurred in phosphate biosorption. In conclusion, woody sawdust is a promising ligno-cellulosic biomaterial used for the removal of phosphate from water as biosorption process. So, the application of nanoscale sawdust particles in wastewater or wastewater-irrigated soils would substantially decrease P runoff and eutrophication. Moreover, the P-enriched nSD-KF can be used as a supplemental P-fertilizer required for plant growth to overcome high cost of mineral fertilizers applied to the agricultural soils.

References

[1] H. Yu, G.H. Covey, A.J. O'Connor, Silvichemicals from pulp mill wastes-biosorption of metal ions on ellagic acid, Appita J., 2 (2000) 559–566.
[2] Q. Du, S. Liu, Z. Cao, Y. Wang, Ammonia removal from aqueous solution using natural Chinese clinoptilolite, Sep. Purif. Technol., 44 (2005) 229–234.
[3] O. Lahav, M. Green, Ammonium removal using ion exchange and biological regeneration, Water Res., 32 (1998) 2019–2028.
[4] S. Farag, M.H. Abo-Shosha, N.A. Ibrahim, Application of starch ion exchange composites II. Removal of some acid dyestuffs using starch methylenbis acrylamide/dimethylaminoethyl methacrylate anion exchange composite, Tinctoria, 10 (1994) 48–56.
[5] K.C. Makris, D. Sarkar, R. Datta, Aluminum-based drinking-water treatment residuals: a novel sorbent for perchlorate removal, Environ. Pollut., 140 (2006) 9–12.
[6] J.M. Novak, D.W. Watts, Increasing the phosphorus sorption capacity of southeastern Coastal Plain soils using water treatment residuals, Soil Sci., 169 (2004) 206–214.
[7] E.A. Elkhatib, A.M. Mahdy, F.K. Sherif, K.A. Salama, A novel sorbent for enhanced phosphorus removal from aqueous medium, Curr. Nanosci., 11 (2015) 655–668.
[8] S. Brunauer, P.H. Emmett, E. Teller, Adsorption of gases in multimolecular layers, J. Am. Chem. Soc., 60 (1938) 309–319.
[9] J.B. Jones Jr., Laboratory Guide for Conducting Soil Tests and Plant Analysis, CRC Press, USA, 2001.
[10] R. Nadeem, T.M. Ansari, A.M. Khalid, Fourier transform infrared spectroscopic characterization and optimization of Pb(II) biosorption by fish (*Labeo rohita*) scales, J. Hazard. Mater., 156 (2008) 64–73.
[11] A.R. Dinçer, Y. Güneş, N. Karakaya, E. Güneş, Comparison of activated carbon and bottom ash for removal of reactive dye from aqueous solution, Bioresour. Technol., 98 (2007) 834–839.
[12] A.R. Binupriya, M. Sathishkumar, S.H. Jung, S.H. Song, S.I. Yun, A novel method in utilization of bokbunja seed wastes from wineries in liquid-phase sequestration of reactive blue 4, Int. J. Environ. Res., 3 (2009) 1–12.
[13] C.H. Giles, D. Smith, A. Huitson, A general treatment and classification of the solute adsorption isotherm. I. Theoretical, J. Colloid Interface Sci., 47 (1974) 755–765.
[14] E.A. Elkhatib, A.M. Mahdy, M.M. ElManeah, Effects of drinking water treatment residuals on nickel retention in soils: a macroscopic and thermodynamic study, J. Soils Sediments, 13 (2013) 94–105.
[15] T.H. Christensen, Cadmium soil sorption at low concentrations: VIII. Correlation with soil parameters, Water Air Soil Pollut., 44 (1989) 71–82.
[16] K. Kadirvelu, K. Thamaraiselvi, C. Namasivayam, Removal of heavy metals from industrial wastewaters by adsorption onto activated carbon prepared from an agricultural solid waste, Bioresour. Technol., 76 (2001) 63–65.
[17] M.S. Rosenthal, J.S. Ross, R. Bilodeau, R.S. Richter, J.E. Palley, E.H. Bradley, Economic evaluation of a comprehensive teenage pregnancy prevention program: pilot program, Am. J. Preventive Med., 37 (2009) S280–S287.
[18] E.A. Elkhatib, J.L. Hern, Kinetics of potassium desorption from Appalachian soils, Soil Sci., 145 (1988) 11–19.
[19] E.A. Elkhatib, O.L. Bennett, R.J. Wright, Kinetics of arsenite sorption in soils [Elovich equation, modified Freundlich equation, sorption mechanism], J. Soil Sci. Soc. Am., 48 (1984) 758–762.
[20] E.A. Elkhatib, G.M. Elshebiny, A.M. Balba, Kinetics of lead sorption in calcareous soils, Arid Land Res. Manage., 6 (1992) 297–310.
[21] S. Kuo, E.G. Lotse, Kinetics of phosphate adsorption and desorption by hematite and gibbsite1, Soil Sci., 116 (1973) 400–406.
[22] M. Özacar, I.A. Şengil, Adsorption of metal complex dyes from aqueous solutions by pine sawdust, Bioresour. Technol., 96 (2005) 791–795.
[23] L.H. Abdel-Rahman, A.M. Abu-Dief, M.A. Abd-El Sayed, M.M. Zikry, Nano sized *Moringa oleifera* an effective strategy for Pb(II) ions removal from aqueous solution, Chem. Mater. Res., 8 (2016) 8–22.
[24] M.A. Wahab, S. Jellali, N. Jedidi, Effect of temperature and pH on the biosorption of ammonium onto *Posidonia oceanica* fibers: equilibrium, and kinetic modeling studies, Bioresour. Technol., 101 (2010) 8606–8615.
[25] H. Gogoi, T. Leiviskä, E. Heiderscheidt, H. Postila, J. Tanskanen, Removal of metals from industrial wastewater and urban runoff by mineral and bio-based sorbents, J. Environ. Manage., 209 (2018) 316–327.
[26] E.A. Ajav, O.A. Fakayode, Physical properties of moringa (*Moringa oleifera*) seeds in relation to an oil expeller design, Agrosearch, 13 (2013) 115–130.
[27] R.L. Mnisi, P.P. Ndibewu, Surface and adsorptive properties of *Moringa oleifera* bark for removal of V(V) from aqueous solutions, Environ. Monit. Assess., 189 (2017) 606–611.

[28] R.J. Hunter, Zeta Potential in Colloid Science-Principle and Applications, Academic Press, New York, NY, 1988, pp. 255–257.

[29] D.J. Shaw, Colloid and Surface Chemistry, Great, Oxford, 1993.

[30] Y. Lin, H. Liu, Zeta potential of a subbituminous coal and its effect on particle agglomeration, Min. Metall. Explor., 13 (1996) 31–35.

[31] N. Abidi, J. Duplay, A. Jada, E. Errais, M. Ghazi, K. Semhi, M. Trabelsi-Ayadi, Removal of anionic dye from textile industries' effluents by using Tunisian clays as adsorbents. Zeta potential and streaming-induced potential measurements, C.R. Chim., 22 (2019) 113–125.

[32] R. Gao, J. Wang, Effects of pH and temperature on isotherm parameters of chlorophenols biosorption to anaerobic granular sludge, J. Hazard. Mater., 145 (2007) 398–403.

[33] V.T. Fávere, H.G. Riella, S.D. Rosa, Chitosan-*n*-2-hydroxypropyl trimethyl ammonium chloride as adsorbent for the removal of the reactive dye from aqueous solutions, Quím. Nova, 33 (2010) 1476–1481.

[34] S. Jellali, M.A. Wahab, M. Anane, K. Riahi, N. Jedidi, Biosorption characteristics of ammonium from aqueous solutions onto *Posidonia oceanica* (L.) fibers, Desalination, 270 (2011) 40–49.

[35] B. Mittal, I, me, and mine—how products become consumers› extended selves, J. Consum. Behav. Int. Res. Rev., 5 (2006) 550–562.

[36] Z. Wang, H. Guo, F. Shen, G. Yang, Y. Zhang, Y. Zeng, L. Wang, H. Xiao, S. Deng, Biochar produced from oak sawdust by Lanthanum (La)-involved pyrolysis for adsorption of ammonium (NH_4^+), nitrate (NO_3^-), and phosphate (PO_4^{3-}), Chemosphere, 119 (2015) 646–653.

[37] J. Huang, N.R. Kankanamge, C. Chow, D.T. Welsh, T. Li, P.R. Teasdale, Removing ammonium from water and wastewater using cost-effective adsorbents: a review, J. Environ. Sci., 63 (2018) 174–197.

[38] P.S. Bryant, J.N. Petersen, J.M. Lee, T.M. Brouns, Sorption of heavy metals by untreated red fir sawdust, Appl. Biochem. Biotechnol., 34 (1992) 777–788.

[39] N.A. Qambrani, M.M. Rahman, S. Won, S. Shim, C. Ra, Biochar properties and eco-friendly applications for climate change mitigation, waste management, and wastewater treatment: a review, Renewable Sustainable Energy Rev., 79 (2017) 255–273.

[40] C. Raji, G.N. Manju, T.S. Anirudhan, Removal of heavy metal ions from water using sawdust-based activated carbon, Indian J. Eng. Mater. Sci., 4 (1997) 254–260.

[41] T.S. Anirudhan, M.K. Sreedhar, Adsorption thermodynamics of Co(II) on polysulphide treated sawdust, Indian J. Chem. Technol., 5 (1998) 41–47.

[42] A.M. Ismail, S.B. Padrick, B. Chen, J. Umetani, M.K. Rosen, The WAVE regulatory complex is inhibited, Nat. Struct. Mol. Biol., 16 (2009) 561–563.

[43] M. Fomina, G.M. Gadd, Biosorption: current perspectives on concept, definition and application, Bioresour. Technol., 160 (2014) 3–14.

[44] R. Gnanasambandam, A. Proctor, Determination of pectin degree of esterification by diffuse reflectance Fourier transform infrared spectroscopy, Food Chem., 68 (2000) 327–332.

[45] G. Crini, Recent developments in polysaccharide-based materials used as adsorbents in wastewater treatment, Prog. Polym. Sci., 30 (2005) 38–70.

[46] A. Ronda, M. Della Zassa, M.A. Martin-Lara, M. Calero, P. Canu, Combustion of a Pb(II)-loaded olive tree pruning used as biosorbent, J. Hazard. Mater., 308 (2016) 285–293.

[47] B. Volesky, Sorption and Biosorption. BV Sorbex Inc., St. Lambert, Quebec, 2003, p. 326.

[48] A.M. Mahdy, M.Z.M. Salem, A.M. Ali, H.M. Ali, Optimum operating conditions for the removal of phosphate from water using of wood-branch nanoparticles from *Eucalyptus camaldulensis*, Materials, 13 (2020) 1851.